2023 IEEE International Conference on Robotics and Automation (ICRA 2023)
May 29 - June 2, 2023. London, UK

Increasing Admittance of Industrial Robots By Velocity Feedback Inner-Loop Shaping

Kangwagye Samuel[1,2], Kevin Haninger[2], and Sehoon Oh[1]

Abstract— **Admittance and impedance controllers are often purely feedforward, using measured external force or motion, respectively, to generate a reference for an inner-loop controller. In this case, the range of dynamics which can be rendered is limited by the inner-loop, which causes, e.g. contact stability issues for low admittance industrial robots in stiff contact. When both position and force are measured, feedback control can be added to more flexibly reshape the rendered dynamics. This paper uses velocity feedback to increase the admittance of motion-controlled industrial robots in force control applications. This allows an industrial robot with a lower intrinsic admittance, which may be needed for payload, speed, or accuracy, to realize a higher admittance by control, allowing lighter manual guidance and safer contact. This is achieved by a modified disturbance observer, where an inverse dynamic model estimates external forces and amplifies them with positive feedback. This approach is compared with using positive velocity feedback with a shaping filter. Here, velocity reference calculated by the virtual admittance model is modified by the DOB (Dist-Add) or the positive velocity feedback (Vel-Add). When combined with an outer-loop admittance controller, these methods can render a higher admittance while maintaining contact stability compared to standard feedforward admittance control.**

I. Introduction

Admittance control allows robots to make safe contact by designing and controlling the robot response to external force or motion [1]. By changing the rendered dynamics through control, a single robot hardware can meet a broader range of applications, from safe environment contact [2] to lighter manual guidance [3].

The sensors, actuators, and control architectures used to achieve this vary widely [4]. High admittance (i.e., low stiffness, low inertia) elements can be used for the human interface [5] or actuators [6]. A high intrinsic admittance has the advantage of improved contact stability [4], [7] and reduced peak collision force [8]. However, high admittance robots often have limitations in speed, payload, accuracy, or reach which can be critical in some applications [9], [10].

An industrial robot can be used for interactive control, with a force/torque sensor and an admittance controller that uses virtual mass, damping, and stiffness to produce a desired motion command [4], [11]. This comes at the cost of a lower intrinsic admittance, especially at higher frequencies, causing higher forces in contact transitions [8], [12] and issues with contact stability [13]. To address this, advanced admittance control has been proposed with a range of feedforward controllers to improve contact stability, using a feedforward model of the inverse robot dynamics [13], a PID compensator [2] or a lead controller [10], [11]. However, stability - especially contact stability with a higher stiffness environment - remains a challenge which limits the range of admittance which can be rendered [11].

Most admittance control is feedforward (force measurement to robot motion command), and the use of velocity feedback has been limited. Compensating payload acceleration forces by differentiating robot position measurements increases high-frequency admittance [3], [11], but is often limited by noise [10]. In Natural admittance control [14], arbitrary transfer functions from force and velocity are found based on a model and desired admittance. However, this was only applied to a 1-DOF system.

Measured robot motion can also be used to estimate external force, by using the known inputs and a dynamic model. If the external force is considered as a disturbance, a Disturbance Observer (DOB) [15] can use the measured output, robot model, and known input to estimate the unknown input. The DOB is typically used to directly compensate for the estimated disturbance, which can improve performance on compliant actuators [16]–[18] and high-DOF robots [19], [20]. On high-DOF systems, the momentum observer is often utilized [21], which can be used to implement force control without force measurement [22].

In this paper, we propose using velocity feedback to increase the admittance of industrial robots, towards improving their contact stability with admittance control [16], [23]. Here, the velocity reference calculated by the virtual admittance model is later modified by the proposed methods. Using velocity feedback can offer two advantages. For one, it can be used to estimate external force via a DOB, which can be fed back in a positive amplification, increasing the admittance of the inner-loop controller before an admittance controller is applied. Secondly, positive velocity feedback allows more general loop shaping of the system, which can allow increased sensitivity to human input (low frequency input) while keeping contact stability (transition frequencies $1-5$ Hz). Compared with standard feedforward admittance control, this approach is shown to increase the robot admittance which can be safely rendered.

This paper is organized as follows. Section II discusses the problem, Section III presents the design and analysis of

This work was supported by: the Technology Innovation Programme (20015101) funded by the Ministry of Trade, Industry & Energy (MOTIE, Korea), the National Research Foundation of Korea (NRF) grant funded by the Korea government (MSIP) (NRF-2019R1A2C2011444), and the European Union's Horizon 2020 research and innovation programme under grant agreement No 820689 — SHERLOCK.

[1]Department of Robotics and Mechatronics Engineering, DGIST, Daegu, 42988, Korea [ksamuel27, sehoon]@dgist.ac.kr

[2]Department of Automation, Fraunhofer IPK, Berlin, Germany kevin.haninger@ipk.fraunhofer.de

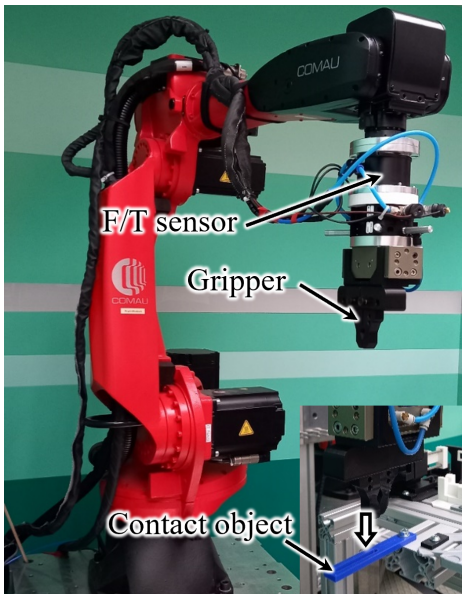

Fig. 1. The COMAU RACER-7-1.4 robot.

the proposed control schemes. Experiments are conducted in Section IV, and the conclusion is given in Section V.

II. Problem Description

This section introduces the models for the robot, standard admittance control, and its limitations.

A. The Robot and its Basic Admittance Control Architecture

The target system is a manipulator with a fixed inner-loop position/velocity controller presented in Fig. 1. A 6-DOF force/torque (F/T) sensor is coupled to the robot flange, and the gripper is then rigidly fixed to the F/T sensor. External force acts on the robot from the user and/or environment through the gripper, physically acting on the robot dynamics and being measured through the F/T sensor. An inner-loop task space motion controller tracks the motion command supplied by the admittance controller. Admittance control is realized about a compliant frame (typically the robot's Tool Center Point (TCP)), where the total control is diagonal and each DOF is independent. The force measurements are transformed into this frame before payload compensation, and the robot motion is commanded in this frame.

The basic admittance control block diagram of Fig. 1 is shown by the black-solid lines in Fig. 2 for a single DOF in task space. Force can be supplied in two ways: either through the external force, F_{ext}, or the internal force reference, F_r. Note that, the external force, F_{ext}, is composed of human, F_{hum}, and environment, F_{env}, forces. The error from the reference, F_r, and measured forces passes through the virtual admittance controller, $A(s)$, to generate the velocity command, V_i, which is supplied to the closed-loop position/velocity controlled robot with linearized dynamics $R_d(s)$, controller $R_c(s)$, and closed-loop dynamics $R(s)$. This forces the robot to move with velocity, V, and thus, generating the force, F.

The robot model in Fig. 2 is in task space and assumed to be linearized and diagonal (i.e., each task space DOF is

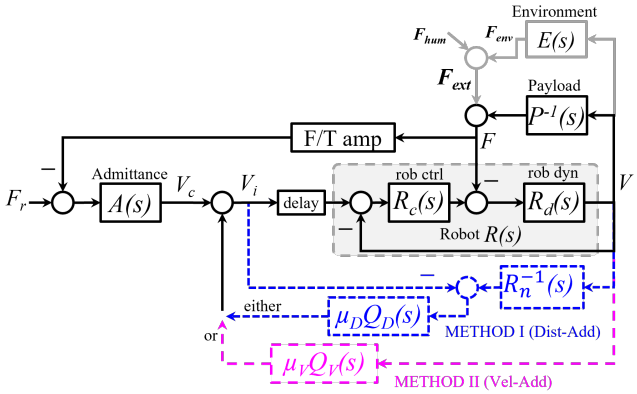

Fig. 2. Admittance control block diagram of the robot in Fig. 1. This includes the basic structure in solid-black lines, and the proposed methods in dashed-blue/mangenta lines.

independent), thus, a single DOF is analyzed in this paper. A linear model allows the use of frequency-domain analysis of contact resonance and rendered admittance, the effectiveness of these assumptions are tested experimentally. The control is applied to the linear Cartesian DOF but not orientation, as the linear motion typically generates larger contact forces. The task space model may change in different robot poses, so model uncertainty is considered in Section III-C. The subsystems in Fig. 2 are considered in a single DOF in Laplace domain as:

$$R_d(s) = \frac{1}{M_r s + B_r},\ P(s) = \frac{1}{M_p s},\ E(s) = \frac{K_e}{s},$$
$$R_c(s) = k_p + \frac{k_i}{s},\ A(s) = \frac{1}{M_a s + B_a}, \tag{1}$$

where M_r and B_r are robot mass and damping, M_p is payload mass, K_e is environment stiffness, k_p and k_i are proportional and integral coefficients, M_a and B_a are virtual admittance mass and damping coefficient, respectively.

Note that the actual and nominal ($\bullet_n$) controller and robot parameter values of $R_c(s)$ and $R_d(s)$ in (1) utilized for theoretical analysis from herein after, unless specified otherwise, are determined as discussed in Section IV-A and given below

$$R_c(s) = 1425 + \frac{38000}{s},\quad R_d(s) = \frac{1}{41.7s + 1000},$$
$$R_{cn}(s) = 475 + \frac{19000}{s},\quad R_{dn}(s) = \frac{1}{20.8s + 500}, \tag{2}$$

while $P(s) = 1/2s$, i.e., considering a 2 kg payload mass.

B. Limitation of the Basic Admittance Control System

Let the admittance transfer function from F to V of Fig. 2 be defined by $Y(s) = -V/F$. This is also the passivity transfer function and is derived for the basic admittance control method (solid-black lines) as

$$Y^{\text{basic}}(s) = \frac{R_d(s)(1 + A(s)R_c(s))}{1 + R_c(s)R_d(s)}. \tag{3}$$

From (3), increasing the virtual admittance, $A(s)$, increases the admittance at the interaction port. This phenomenon is illustrated in Fig. 3 where the magnitude increases as $A(s)$

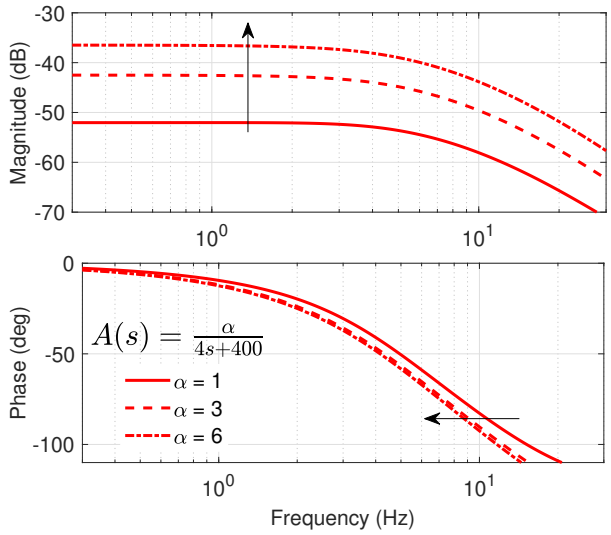

Fig. 3. Bode plot of $Y^{\text{basic}}(s)$ showing the effect of increasing the robot's admittance via virtual admittance parameters.

is scaled by a scalar gain α. However, the phase characteristic shows that increasing the admittance deteriorates the passivity. A system is passive if $\angle Y(s)$ lies between -90^o and 90^o, often used as a stability condition in admittance control [11]. Fig. 3 shows that increasing admittance results in passivity violation at lower frequencies, which often leads to high resonance in contact [24], [25]. This limits the ability to render a high admittance from the virtual admittance parameters alone.

It is hypothesized in this paper that if the inner-loop admittance increases without over compromising the inner-loop motion tracking, the passivity characteristics of the outer loop admittance controller can improve. Thus, the methodologies for increasing the inner-loop admittance are proposed, analyzed, and validated in the sections that follow.

III. Methods For Increasing Admittance

To increase the admittance without deteriorating passivity or contact stability, two methods are proposed to enhance the position/velocity control loop. With these methods, the inner-loop admittance is increased without changing the virtual admittance parameters. Both methods amplify the robot velocity command by utilizing the robot's output velocity in a positive feedback way with loop shaping.

A. Method I: Inner-Loop Disturbance Addition (Dist-Add)

The first method, denoted as 'Dist-Add', is based on estimating external disturbances to the robot motion by using the measured output, an inverse model, and the measured input, as typical in the Disturbance Observer [15]. However, instead of cancelling these estimated disturbances, they are scaled and added to the robot velocity input to amplify the external force, as shown by the dashed-blue lines in Fig. 2. Types of disturbances typically considered for industrial manipulators are high friction, mechanical vibrations due higher-order dynamics, and coupling between degrees of freedom in task space due to imperfections in joint-level control. Here, we also consider that the external forces act

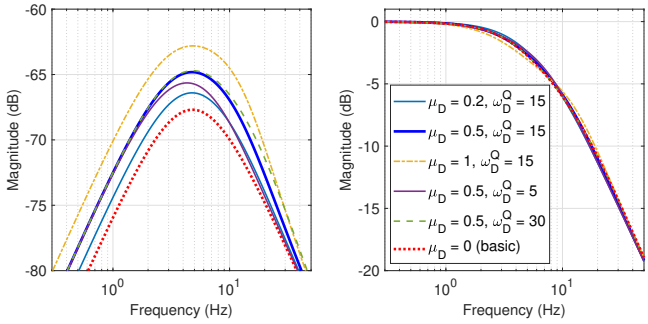

(a) $|V/F|$ (b) $|V/V_c|$

Fig. 4. Magnitude bode plots of transfer functions from F to V and V_c to V when Dist-Add method is utilized, considering only the inner velocity loop i.e., without the admittance loop.

on the robot system, causing deviation from expected motion control performance. From Fig. 2, μ_D is a constant gain for shaping the amount of disturbances to be added, $R_n(s)$ is the nominal model of the inner-loop robot dynamics, $R(s)$, and $Q_D(s)$ is the Q-filter designed as a first-order LPF to make $R_n(s)$ proper as shown below

$$R_n(s) = \frac{R_{cn}(s)R_{dn}(s)}{1 + R_{cn}(s)R_{dn}(s)} \quad \text{and} \quad Q_D(s) = \frac{\omega_D^Q}{s + \omega_D^Q}, \quad (4)$$

where ω_D^Q is the Q-filter cutoff frequency.

The main difference from the conventional disturbance calculation methods [26]–[28] is that the Dist-Add method amplifies the estimated disturbances, instead of cancelling them. This is because the goal here is not precise motion control, but to increase the responsiveness to external forces.

Considering the inner velocity control loop of Fig. 2, the output velocity for Dist-Add is given by

$$\mathcal{V}(s) = \frac{-R_d(s)(1 + \mu_D Q_D(s))}{\xi_1^{\text{Dist-Add}}(s)}\mathcal{F}(s) + \frac{R_c(s)R_d(s)}{\xi_1^{\text{Dist-Add}}(s)}\mathcal{V}_c(s), \quad (5)$$

representing the inner-loop admittance (V/F) and velocity tracking (V/V_c) transfer functions, where

$$\begin{aligned}\xi_1^{\text{Dist-Add}}(s) =& (1 + R_c(s)R_d(s))(1 + \mu_D Q_D(s)) \\ & - R_c(s)R_d(s)\mu_D Q_D(s)R_n^{-1}(s). \quad (6)\end{aligned}$$

When there is no model uncertainty, i.e., $R_n(s) = R(s)$, (6) becomes $\xi_1^{\text{Dist-Add}}(s) = 1 + R_c(s)R_d(s)$. Thus, Dist-Add method does not affect the velocity tracking performance in the absence of model uncertainty. The effect of physical force on the robot and the velocity tracking magnitude plots for (5) are presented in Fig. 4 when μ_D and ω_D^Q vary. It can be observed that with the proposed method, the inner-loop admittance is increased (left) as μ_D increases, whereas the shaping filter cutoff frequency, ω_D^Q, changes the frequency range where admittance is increased. This improvement has a negligible effect on the velocity tracking performance (right) when model uncertainty is as given in (2).

B. Method II: Inner-Loop Positive Velocity Feedback With Shaping Filter (Vel-Add)

The second method of increasing the admittance, denoted as 'Vel-Add', is the positive feedback of the robot velocity

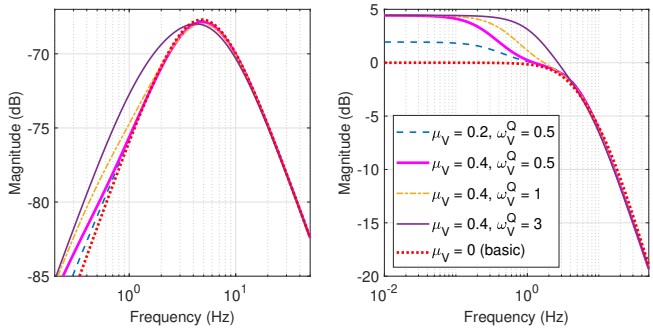

(a) $|V/F|$ (b) $|V/V_c|$

Fig. 5. Magnitude bode plots of transfer functions from F to V and V_c to V when Vel-Add method is utilized, considering the inner velocity loop.

as shown in dashed-magenta lines in Fig. 2. This feedback increases the effective magnitude of the robot response V/F. The key design feature in this method is the velocity shaping filter, which is the product of the gain, μ_V, and the Q-filter, $Q_V(s)$, where μ_V shapes the signal strength and $Q_V(s)$ shapes the loop frequency. $Q_V(s)$ is designed as a first-order LPF as shown below

$$Q_V(s) = \frac{\omega_V^Q}{s + \omega_V^Q}, \tag{7}$$

where ω_V^Q is its cutoff frequency. Since the low frequency admittance dominates the human effort in manipulation, and a high medium frequency admittance (e.g. $1-5$ hz) can affect contact stability, ω_V^Q can be set small to limit the frequency range where the rendered admittance is increased.

Considering the inner velocity control loop of Fig. 2 for Vel-Add, the effect of force on the robot (admittance) and the velocity tracking transfer functions are given by

$$\mathcal{V}(s) = \frac{-R_d(s)}{\xi_1^{\text{Vel-Add}}(s)}\mathcal{F}(s) + \frac{R_c(s)R_d(s)}{\xi_1^{\text{Vel-Add}}(s)}\mathcal{V}_c(s), \tag{8}$$

where $\xi_1^{\text{Vel-Add}}(s)$ is given by

$$\xi_1^{\text{Vel-Add}}(s) = 1 + R_c(s)R_d(s)(1 - \mu_V Q_V(s)). \tag{9}$$

It can be observed from (9) that, positive velocity feedback adds low-frequency gain to the velocity control. Moreover, more frequency shaping is possible than with virtual admittance parameters. The magnitude bode plots of (8) presented in Fig. 5 when μ_V and ω_V^Q are varying show that the low frequency inner-loop admittance (physical F to V without virtual admittance) can be increased with the Vel-Add method. However, in comparison to the Dist-Add method, velocity tracking performance is affected by the low frequency gain. This is advantageous in the sense of ease of robot manipulation by human as long as the desired stability and passivity conditions are not violated.

C. Admittance Control Analysis

The performance and stability of these methods will now be analyzed. In the following analyses, $M_a = 4$, $\mu_D = 0.5$, $\omega_D^Q = 15$ Hz, $\mu_V = 0.4$, and $\omega_V^Q = 0.5$ Hz.

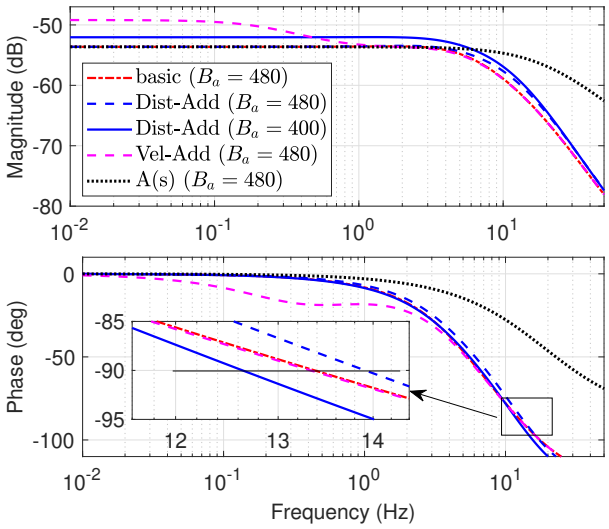

Fig. 6. Bode plot for transfer function $Y(s)$ where $A(s) = 1/(M_a s + B_a)$.

1) Admittance and Passivity Analysis: The admittance transfer functions, $Y(s)$, for both methods in Fig. 2 are derived as shown below

$$Y^{\text{Dist-Add}}(s) = \frac{R_d(s)(1 + \mu_D Q_D(s) + A(s)R_c(s))}{\xi_1^{\text{Dist-Add}}(s)}, \tag{10}$$

$$Y^{\text{Vel-Add}}(s) = R_d(s)(1 + A(s)R_c(s))/\xi_1^{\text{Vel-Add}}(s). \tag{11}$$

The bode plots of (10) and (11) are presented in Fig. 6. With same values of virtual damping coefficient, $B_a = 480$, the Dist-Add method tracks the virtual admittance since their DC gains are equal, i.e., $1/B_a$. On the other hand, Vel-Add increases admittance in the low frequency region since its DC gain is higher, i.e., $1/B_a(1 - \mu_V)$. This shows higher responsiveness to low-frequency external forces due to the addition of low frequency gain and the increased low frequency inner-loop admittance (physical F to V without virtual admittance). However, it can be observed from the phase characteristics that the Dist-Add method improves the passivity/contact stability more compared to the Vel-Add method. Note that, passivity condition is met when the phase lies between 90^o and -90^o. Taking advantage of this passivity improvement, admittance of the Dist-Add method can be increased while sacrificing its phase margin. This is illustrated in Fig. 6 when the Dist-Add method in (10) is plotted with $B_a = 400$, where the admittance has been increased and passivity is violated at a lower frequency.

2) Force Tracking During Contact With Stiff Environment: The force tracking during contact, defined by the transfer function from F_r to F as $H(s) = F/F_r$ is derived for all the control methods as

$$H(s) = R_c(s)R_d(s)A(s)\xi_4(s)/\xi_2(s), \tag{12}$$

where $\xi_2^{\text{Dist-Add}}(s) = \xi_3(1 + \mu_D Q_D) + R_c R_d(A\xi_4 - \mu_D Q_D R_n^{-1})$, $\xi_2^{\text{Vel-Add}}(s) = \xi_3 + R_c R_d(A\xi_4 - \mu_V Q_V)$, $\xi_3(s) = 1 + R_c R_d + R_d \xi_4$, and $\xi_4(s) = P^{-1} + E$.

The magnitude of (12) is plotted in Fig. 7 when the environment stiffness $K_e = 20$ N/mm with the same B_a values as in Fig. 6. When B_a is the same for all, Dist-Add

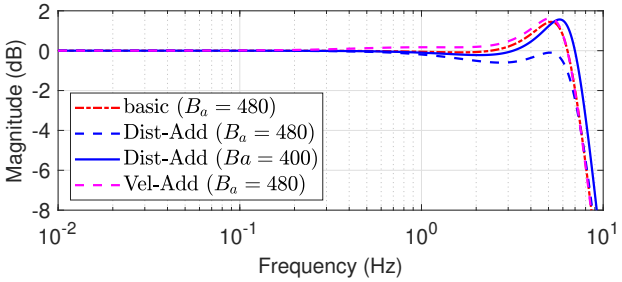

Fig. 7. Bode magnitude plot for $H(s)$ when $K_e = 20$ N/mm.

has the lowest resonance peak as compared to basic and Vel-Add methods. Similarly, when B_a is reduced for the case of Dist-Add method, its resonance peak also increases.

3) Stability Analysis With Dist-Add Method: As in the Disturbance Observer [15], errors between model and plant behavior may cause instability. To examine this, we consider a multiplicative model uncertainty of

$$R(s) = [1 + \Delta(s)]R_n(s), \tag{13}$$

where $\Delta(s)$ is a multiplicative model uncertainty with bounded magnitude. This model uncertainty can describe higher-order dynamics or changes in motion control bandwidth due to changes in robot pose.

To show the stability of the two transfer functions in (5), we assume that the numerators are composed of stable transfer functions, and show that the denominator does not approach 0 for some bound on $|\Delta(s)|$. Applying (13) to the denominator, $\xi_1^{\text{Dist-Add}}(s)$, we factor out $1 + R_cR_d$ to find

$$\begin{aligned}\xi_1^{\text{Dist-Add}}(s) &= (1 + R_cR_d)(1 + \mu_DQ_D - R\mu_DQ_DR_n^{-1}) \\ &= (1 + R_cR_d)(1 - \mu_DQ_D\Delta),\end{aligned} \tag{14}$$

and thus, $|\mu_DQ_D(s)||\Delta(s)| < 1 \ \ \forall s$ is a sufficient condition for stability.

Intuitively, this means that at frequencies where the uncertainty $|\Delta|$ is larger, the force feedback gain μ_DQ_D should be smaller. As one source of model uncertainty is variation in task space motion bandwidth due to changes in robot pose, the bandwidth of Q_D can be set conservatively to meet condition (14). Note that this stability condition is similar to the result for typical DOBs, with the added term μ_D.

IV. Experiments

In this section, experiments involving both robot co-manipulation and autonomous operation are conducted on the COMAU RACER-7-1.4 6-DOF industrial manipulator in Fig. 1 to verify the effectiveness of the proposed control methods. An ME-Meßsysteme KD6110 F/T sensor is fixed to the robot flange and the gripper attached to the F/T sensor with the aid of a rigid coupling.

A. Controller and Robot Parameter Determination

The controller and robot dynamics parameters are experimentally determined by a nonparametric system identification technique. Under position control, a Schroeder multisine, which is utilized as an excitation signal, is supplied as the desired position in Z-axis motion and the position response of the robot in Z-direction is measured by the encoders. These measurements and the command signal are differentiated using a LPF with high cutoff frequency to obtain velocities from which an empirical transfer function is calculated. The model $R_c(s)R_d(s)/(1 + R_c(s)R_d(s))$ is then fit to obtain the values utilized in theoretical analyses as shown in (2). Parameters utilized for controller implementation in experiments are empirically tuned as $R_n(s) = (100s+800)/(2.5s^2+140s+800)$, $\mu_D = 0.5$, $\omega_D^Q = 15$ Hz, $\mu_V = 0.4$, and $\omega_V^Q = 0.5$ Hz, unless specified.

B. Controller Implementation

Since the COMAU RACER robot software platform accepts position commands, the transfer functions in Fig. 2 are translated to produce position commands as

$$X_i^{\text{b}}(s) = \frac{A(s)}{s}\left[\mathcal{F}_r(s) - \mathcal{F}_m(s)\right], \tag{15}$$

$$X_i^{\text{Dist-Add}}(s) = \frac{1}{1 + \mu_DQ_D}X_i^{\text{b}}(s) + \frac{\mu_DQ_DR_n^{-1}}{s(1 + \mu_DQ_D)}\mathcal{V}_m(s), \tag{16}$$

$$X_i^{\text{Vel-Add}}(s) = X_i^{\text{b}}(s) + \frac{\mu_VQ_V(s)}{s}\mathcal{V}_m(s). \tag{17}$$

For faster implementation and tuning between test cycles, the transfer functions in (15), (16), and (17) are discretized with a Tustin transformation in MATLAB at a sample time of 0.0008 s and the result is sent, using the `rosparam` command of the ROS package in MATLAB, to the robot external controller where they are executed in real-time.

C. Contact With Stiff Environment Experiments

The force control performance in contact is examined in making contact with a pure stiffness environment. A 3D-printed beam is cantilevered into the robot's workspace as shown in Fig. 1, and the robot is, starting from a constant position, commanded with a constant F_r to bring the robot into contact with the beam (7.6 N/mm stiff). The force control performance is compared in the sense of peak contact force, settling time, and steady-state force tracking performance, all of which are desired to be reduced.

1) Exp. 1: In the first experiment, the virtual admittance damping parameter for all the methods are normalized such that the robot's speed before contact is same for all the methods. This implies that constant velocity before contact is similar for all the methods. A constant $F_r = 8$ N is supplied and the results are presented in Fig. 8. Dist-Add exhibits the smallest overshoot but slower settling time. On the other hand, Vel-Add shows the largest overshoot, however, the damping is much better at steady-state.

2) Exp. 2: In the second experiment, a larger F_r is supplied. As the Vel-Add has a higher low-frequency admittance, a larger F_r results in too large of a contact velocity with a corresponding large force overshoot in contact, so it is omitted from the high force comparison. The results for basic and Dist-Add methods are presented in Fig. 9. In Fig. 9(a), the same parameters (M_a and B_a) are used and a reduction in overshoot on the Dist-Add can be seen, at the cost of a

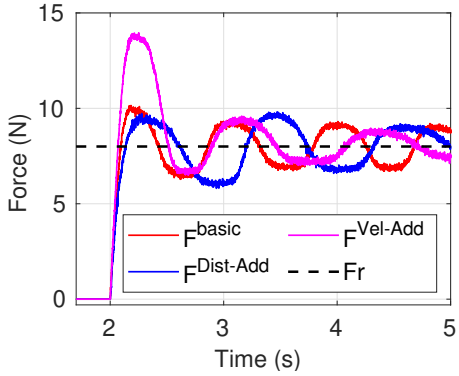

Fig. 8. Contact control results when all the methods are normalized with same resultant admittance gain.

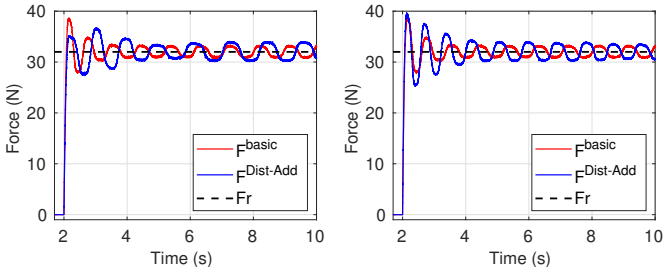

(a) (b)

Fig. 9. Contact control results when larger F_r is supplied. basic: $B_a = 480$ in both while (a) Dist-Add: $B_a = 480$ and $\mu_D = 1$ and (b) Dist-Add: $B_a = 400$ and $\mu_D = 0.5$

longer settling time. When decreasing admittance damping to $B_a = 400$, a comparable overshoot is achieved, showing Dist-Add can allow a reduction in admittance parameters (M_a and B_a) at equivalent peak contact force.

D. Admittance Rendering Experiments

To validate the admittance rendering in free-space, the gripper of the admittance-controlled robot is fastened to a second robot with a large velcro loop as shown in Fig. 10. A motion program is executed on the second robot, leading to repeatable force application on the admittance-controlled robot. By using a high acceleration and high jerk motion profile, the step response characteristics of the admittance controller can be approximately evaluated.

1) Fast motion: The resulting force from the experimental robot under the same velocity profile from the leading robot is shown in Fig. 11. In Fig. 11(a), all controllers are compared at the same admittance parameters (M_a and B_a), and the improvement in the low frequency admittance of Vel-Add can be seen by the lower force induced to achieve the supplied velocity. The basic and Dist-Add methods have comparable average force, but the Dist-Add has slightly higher variance, as the robot disturbances (e.g., nonlinear friction, gear cogging) are also amplified. In Fig. 11(b), the Dist-Add has a $\mu_D = 0.5$, which reduces the variance in steady-state force tracking as the disturbances are not amplified as strongly. Additionally, the $B_a = 400$ for Dist-Add method is compared, as $B_a = 400$ gave comparable contact peak force to basic method with $B_a = 480$. A reduction in the free-space force can be seen, showing the improved ease in manipulation in free space.

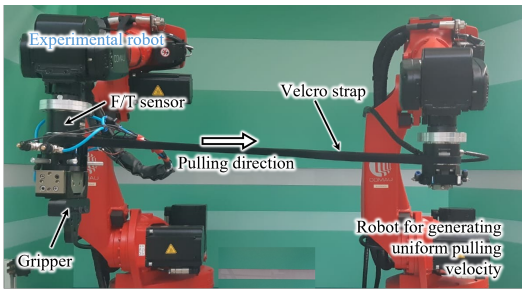

Fig. 10. Setup of robots for admittance rendering experiments.

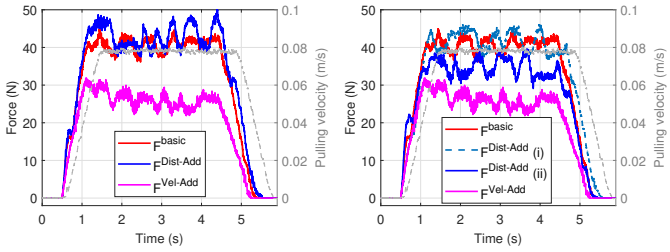

(a) (b)

Fig. 11. Pulling the robot with fast speed. For basic and Vel-Add: $B_a = 480$ and $\mu_V = 0.4$. For Dist-Add: (a) $B_a = 480$ and $\mu_D = 1$ (b) Dist-Add (i): $B_a = 480$ and $\mu_D = 0.5$, Dist-Add (ii): $B_a = 400$ and $\mu_D = 0.5$

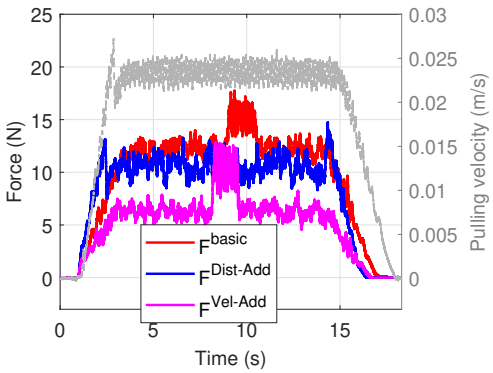

Fig. 12. Pulling the robot with slow speed. basic: $B_a = 480$, Dist-Add: $B_a = 400$ and $\mu_D = 0.5$. Vel-Add: $B_a = 480$ and $\mu_V = 0.4$

2) Slow motion: In these tests, a velocity reference of 2.5 cm/sec instead of 8 cm/sec is applied. The results can be seen in Fig. 12, where the Vel-Add again achieves a much lower required force. The Dist-Add has slightly reduced the mean force required, but the change is not significant as the Dist-Add does not change the low-frequency admittance (see, e.g., Fig. 6).

V. Conclusions

This paper has shown that the admittance of an industrial robot can be safely increased with velocity feedback. Estimating external force with a disturbance observer and amplifying it decreases the force peak in contact transitions, and can allow the admittance to be safely increased while keeping a maximum collision force. This has the trade-off of amplifying other disturbances, reducing the steady-state tracking accuracy of the robot. The positive velocity feedback can increase the low-frequency admittance, which leads to higher contact velocities and a higher collision peak. However, the settling time in contact and free-space admittance are improved.

REFERENCES

[1] N. Hogan, "Impedance Control: An Approach to Manipulation: Part II—Implementation," *J. Dyn. Sys., Meas., Control*, vol. 107, pp. 8–16, Mar. 1985.

[2] H. Cao, Y. He, X. Chen, and X. Zhao, "Smooth adaptive hybrid impedance control for robotic contact force tracking in dynamic environments," *Industrial Robot: the international journal of robotics research and application*, vol. 47, pp. 231–242, Jan. 2020.

[3] S. Farsoni, C. T. Landi, F. Ferraguti, C. Secchi, and M. Bonfe, "Compensation of load dynamics for admittance controlled interactive industrial robots using a quaternion-based kalman filter," *IEEE Robotics and Automation Letters*, vol. 2, no. 2, pp. 672–679, 2017.

[4] A. Calanca, R. Muradore, and P. Fiorini, "A Review of Algorithms for Compliant Control of Stiff and Fixed-Compliance Robots," *IEEE/ASME Transactions on Mechatronics*, vol. 21, pp. 613–624, Apr. 2016.

[5] J.-M. Audet and C. Gosselin, "Intuitive Physical Human-Robot Interaction using an Underactuated Redundant Manipulator with Complete Spatial Rotational Capabilities," *Journal of Mechanisms and Robotics*, pp. 1–15, May 2021.

[6] G. Pratt and M. Williamson, "Series elastic actuators," in *1995 IEEE/RSJ International Conference on Intelligent Robots and Systems 95. 'Human Robot Interaction and Cooperative Robots', Proceedings*, vol. 1, pp. 399–406 vol.1, Aug. 1995.

[7] S. D. Eppinger and W. P. Seering, "Three dynamic problems in robot force control," *IEEE Transactions on Robotics and Automation*, vol. 8, no. 6, pp. 751–758, 1992.

[8] S. Haddadin, A. De Luca, and A. Albu-Schäffer, "Robot Collisions: A Survey on Detection, Isolation, and Identification," *IEEE Transactions on Robotics*, vol. 33, pp. 1292–1312, Dec. 2017.

[9] P. Franceschi, N. Castaman, S. Ghidoni, and N. Pedrocchi, "Precise Robotic Manipulation of Bulky Components," *IEEE Access*, vol. 8, pp. 222476–222485, 2020.

[10] K. Haninger, M. Radke, A. Vick, and J. Kruger, "Towards High-Payload Admittance Control for Manual Guidance with Environmental Contact," *IEEE Robotics and Automation Letters*, 2022.

[11] A. Q. Keemink, H. van der Kooij, and A. H. Stienen, "Admittance control for physical human–robot interaction," *The International Journal of Robotics Research*, vol. 37, pp. 1421–1444, Sept. 2018.

[12] K. Haninger and D. Surdilovic, "Bounded Collision Force by the Sobolev Norm: Compliance and Control for Interactive Robots," in *2019 IEEE International Conference on Robotics and Automation (ICRA)*, pp. 8259–8535, 2019.

[13] D. Surdilovic, "Robust control design of impedance control for industrial robots," in *Intelligent Robots and Systems, 2007. IROS 2007. IEEE/RSJ International Conference On*, pp. 3572–3579, IEEE, 2007.

[14] W. S. Newman and Y. Zhang, "Stable interaction control and coulomb friction compensation using natural admittance control," *Journal of robotic systems*, vol. 11, no. 1, pp. 3–11, 1994.

[15] K. Ohnishi, M. Shibata, and T. Murakami, "Motion control for advanced mechatronics," *Mechatronics, IEEE/ASME Transactions on*, vol. 1, no. 1, pp. 56–67, 1996.

[16] S. Oh, K. Kong, and Y. Hori, "Design and analysis of force-sensor-less power-assist control," *IEEE Transactions on Industrial Electronics*, vol. 61, no. 2, pp. 985–993, 2013.

[17] N. Paine, J. S. Mehling, J. Holley, N. A. Radford, G. Johnson, C.-L. Fok, and L. Sentis, "Actuator Control for the NASA-JSC Valkyrie Humanoid Robot: A Decoupled Dynamics Approach for Torque Control of Series Elastic Robots," *Journal of Field Robotics*, vol. 32, no. 3, pp. 378–396, 2015.

[18] S. Oh and K. Kong, "High-precision robust force control of a series elastic actuator," *IEEE/ASME Transactions on mechatronics*, vol. 22, no. 1, pp. 71–80, 2016.

[19] E. Sariyildiz, H. Sekiguchi, T. Nozaki, B. Ugurlu, and K. Ohnishi, "A stability analysis for the acceleration-based robust position control of robot manipulators via disturbance observer," *IEEE/ASME Transactions on Mechatronics*, vol. 23, no. 5, pp. 2369–2378, 2018.

[20] K. Samuel, K. Haninger, and S. Oh, "High-performance admittance control of an industrial robot via disturbance observer," in *IECON 2022–48th Annual Conference of the IEEE Industrial Electronics Society*, pp. 1–6, IEEE, 2022.

[21] A. De Luca and R. Mattone, "Sensorless robot collision detection and hybrid force/motion control," in *Proceedings of the 2005 IEEE International Conference on Robotics and Automation*, pp. 999–1004, IEEE, 2005.

[22] M. Geravand, F. Flacco, and A. De Luca, "Human-robot physical interaction and collaboration using an industrial robot with a closed control architecture," in *Robotics and Automation (ICRA), 2013 IEEE International Conference On*, pp. 4000–4007, IEEE, 2013.

[23] S. Oh, H. Woo, and K. Kong, "Frequency-shaped impedance control for safe human–robot interaction in reference tracking application," *IEEE/ASME Transactions On Mechatronics*, vol. 19, no. 6, pp. 1907–1916, 2014.

[24] S. P. Buerger and N. Hogan, "Relaxing Passivity for Human-Robot Interaction," in *2006 IEEE/RSJ International Conference on Intelligent Robots and Systems*, pp. 4570–4575, Oct. 2006.

[25] K. Haninger and M. Tomizuka, "Robust passivity and passivity relaxation for impedance control of flexible-joint robots with inner-loop torque control," *IEEE/ASME Transactions on Mechatronics*, vol. 23, no. 6, pp. 2671–2680, 2018.

[26] K. Ohnishi, M. Shibata, and T. Murakami, "Motion control for advanced mechatronics," *IEEE/ASME transactions on mechatronics*, vol. 1, no. 1, pp. 56–67, 1996.

[27] W.-H. Chen, J. Yang, L. Guo, and S. Li, "Disturbance-observer-based control and related methods—an overview," *IEEE Transactions on industrial electronics*, vol. 63, no. 2, pp. 1083–1095, 2015.

[28] Y. Yokokura and K. Ohishi, "Fine load-side acceleration control based on torsion torque sensing of two-inertia system," *IEEE Transactions on Industrial Electronics*, vol. 67, no. 1, pp. 768–777, 2018.